9th International Conference on Numerical Ship Hydrodynamics
Ann Arbor, Michigan, August 5-8, 2007

Computation of transom-stern flows using a steady free-surface fitting RANS method

Bram Starke, Hoyte Raven, Auke van der Ploeg
(Maritime Research Institute Netherlands (MARIN))

ABSTRACT

This paper discusses a detailed computational study of the flow off a 2D transom stern. The steady RANS solver PARNASSOS is used, using a surface-fitting technique and the steady iterative solution algorithm for the free surface.

For dry-transom flow, 'inviscid' computations using this RANS solver show excellent agreement with nonlinear potential-flow solutions available in the literature. Viscous effects are shown to cause a substantial reduction of the trailing wave length, and a scale effect on that wave length. The transom immersion is systematically increased to investigate the limits of the dry-transom regime. A local vanishing of the longitudinal velocity at the wave surface near the first wave crest is used as an indication of wave breaking. The critical Froude number at which this happens is substantially increased by viscous effects, and much more so for model scale than for full scale. Therefore, in a range of transom Froude numbers a smooth flow will occur at full scale, but a spilling breaker just aft of the transom at model scale. It is shown that the width of this range may depend on the hull form, as it results from two opposite scale effects.

For wetted transom flows, the predictions at model scale show good agreement with experimental data for the water level at the transom and the trailing wave system. The transom immersion is systematically decreased to investigate the clearance of the transom. It is shown that at a given transom immersion the clearance is larger at full scale than at model scale. Thus there is a range of conditions where the transom is just cleared at full scale, with a spilling breaker downstream, while the flow is still attached to the transom at model scale.

INTRODUCTION

Methods to compute viscous flows with free surface around ship hulls have undergone substantial development over the last decade. While most current methods ask large computation times, and dense grids are needed to avoid undue numerical wave damping, the limits are being gradually shifted and practical application in ship design is approaching.

Today, the most common way to predict ship wave patterns and wave resistance in practical ship design is by using free-surface potential flow codes. Compared with these, the much more computationally-intensive RANS/FS codes include all viscous effects on the wave pattern; therefore, should offer improved stern wave predictions in the first place, and perhaps other improvements locally; besides, of course, providing the viscous flow field.

An important application area in which RANS/FS codes should enable a step forward in design quality is the flow off a transom stern. The majority of modern vessels has a transom stern, which is immersed at rest for fast vessels and for some very full-block vessels, but which usually is above the still-water surface for most merchant ships. Design requirements have stimulated the use of very wide and flat transom sterns, e.g. for ferries. Thus the design of the stern and choice of the transom edge height has become rather critical; in particular since an improperly designed wide transom tends to generate transverse waves which are detrimental for resistance.

For a proper transom stern design, it is essential to foresee the flow regime that will occur there: will the transom be wetted or dry, for the ship at full scale at a given draft and speed? Will the flow be smooth or will wave breaking occur aft of the transom? It is not easy to answer that question based on experience only. Rules-of-thumb are sometimes quoted for assessing whether a transom is cleared, e.g. Saunders (1957); but these are based on a transom Froude number which does not even exist for a transom above the still-water surface. These simple rules are only applicable in very simple situations and are evidently inadequate for normal ships. In general situations, the transom flow regime depends on the transom height and shape, buttock slope, the wave system generated upstream, the boundary layer flow around the hull, etc. Therefore, RANS/FS methods can make an important contribution by predicting the transom flow pattern, and enabling a more precise stern design to guarantee a favourable flow at full scale.

The present paper describes a detailed study to evaluate the accuracy and applicability of such predictions. Also, it addresses the viscous and scale effects on the flow pattern aft of the transom, which appear to be remarkable. Since the RANS code used is a steady surface-fitting method, it does not include all the physics occurring, such as wave breaking or unsteadiness. Therefore, an additional objective of the study is to assess the practical applicability of such a method to the various transom flow regimes.

The paper is set up as follows. The next section describes the main physics of transom flows, and reviews existing literature; leading to the questions to be addressed in this paper. Subsequently we briefly describe the computational method we use, followed by a description of the test case. Next, the dry-transom regime, the intermediate regime (characterised by wave breaking just aft of the transom) and the wetted-transom regime are addressed discussing detailed studies for the simplified 2D test case. Then a discussion of transom resistance and a simplified model to understand some of the physics in the wetted flow regime are followed by a brief discussion of the extension to 3D cases and finally the conclusions drawn from the present investigation.

TRANSOM-STERN FLOWS

Physics

We shall first concisely describe the principal physics playing a role in transom flows. Conventionally, a distinction is made between a dry transom flow and a wetted transom flow. In the dry-transom regime, the water surface leaves the transom edge more or less smoothly. This requires that the pressure at the transom edge equals the ambient (atmospheric) pressure. If the hull would just continue smoothly aft instead of being cut off at the transom edge, the pressure level there would in most cases be higher than the ambient pressure; dependent on the aftbody shape, the ship wave pattern, propeller action etc. The transom flow must then be such as to cancel that pressure difference. This means that the flow will curve upward, the convexity of the streamlines producing the required pressure decrease. A wave crest aft of the transom will occur. For increasing transom immersion, the required pressure reduction increases, and so does the upward curvature and the resulting stern wave height.

In inviscid flow, Bernoulli's equation connects the wave elevation and the velocity of the flow at the surface. Maximum wave height, and maximum wave resistance, occurs for a transom immersion such that the flow velocity vanishes at the wave crest. For larger immersions (or lower speeds), no dry-transom solution is possible in an inviscid flow without wave breaking.

In a viscous flow, however, there is a boundary layer along the hull, which leaves the hull at the transom edge. The resulting wake that remains along the wave surface has a momentum deficit compared with the inviscid flow. Consequently, as this wake has to flow against gravity towards the first wave crest, for sufficiently steep waves (less than the limiting steepness in inviscid flow) the velocity will vanish at some point, which is an indication of the onset of wave breaking. A spilling wave breaker will occur at the front face of the first wave crest aft of the transom. For increasing transom immersion, the vanishing of the velocity will occur closer to the transom, until at some point the spilling breaker reaches the transom and forms a recirculation region aft of the transom, giving rise to the wetted-transom regime.

In the wetted-transom regime, in this recirculation region aft of the wetted part of the transom the pressure is reduced, therefore the water surface is somewhat below the surrounding level. When the transom immersion is reduced or the speed increased, this depression reaches the transom edge again, and the reverse transition to a dry-transom flow can follow. Through this transition the flow is strongly unsteady (Maki et al, 2006).

As mentioned, a main parameter determining the transom flow is the pressure level that would prevail at the position of the transom edge in case the hull would just be extended aft; to be denoted Δcp_{tr} . In case any effects of the hull form and wave system can be neglected (as is valid for the 2D semi-infinite body considered later), this is just the hydrostatic pressure at the transom edge, in nondimensional form:

$$\Delta cp_{tr} = 2 Fn_{tr}^{-2}$$

in which $Fn_{tr} = V / \sqrt{g.T_{tr}}$ is the transom immersion Froude number and T_{tr} is the transom draft. In such cases Fn_{tr} is the main parameter determining the flow; but in more general cases it is not. While the pressure difference Δcp_{tr} is more meaningful in general, it does not provide any simple design rule.

Literature review

There is quite some literature on the computation of transom flows, but mostly for potential-flow methods. For the earlier linearised free-surface potential-flow methods, modelling transom flows remained insatisfactory, as the requirement that the wave surface leaves the hull at the transom edge, in most cases is inconsistent with the linearisation assumptions. For flat-ship linearised methods, a consistent treatment is possible, and an important paper on this by Schmidt (1981) points out several properties of transom flows,

e.g. the presence of a square-root singularity of the pressure along the hull at the transom edge.

Nonlinear free-surface potential-flow methods, however, do admit an adequate modelling of the dry-transom regime. A most significant paper on the fundamentals of transom flows is Vanden-Broeck (1980). He considers a 2D semi-infinite body with a flat bottom and transom, and derives accurate fully nonlinear potential flow solutions for dry-transom flows. Vanden-Broeck demonstrated that at a critical value of $Fn_{tr} = 2.23$, the trailing wave system reaches maximum height, and for lower Fn_{tr} no potential-flow solution of dry-transom flow exists. Scorpio & Beck (1997) address the same case, but use a more general singularity method, getting solutions in good agreement with Vanden-Broeck's results. Similarly, the widely used 3D panel codes to solve the fully nonlinear problem can reproduce this solution fairly well, and in practice give very useful indications on dry-transom flows (Raven, 1998). However, they are unable to predict wetted-transom flows or indicate which of the regimes occurs due to the neglect of viscous and wave breaking effects.

Much more complete representations can be expected from RANS/FS methods, as these do include the interplay between viscous and free-surface effects. An early paper is Haussling et al (1997), who show some fairly good predictions for the 5415 case at $Fn = 0.41$, indicating that in viscous flow the stern wave is noticeably further forward than in inviscid flow. At the Gothenburg 2000 workshop, rather variable predictions were shown for the 5415 model at $Fn = 0.28$; but no specific information was given on the treatment or accuracy. Lin and Percival (2001) discuss a grid topology for a surface-fitting method that would permit to model the transition between a wetted and a dry-transom regime, but their predictions show no illustration that this is achieved. At the CFD Workshop Tokyo 2005, large variations in the stern wave pattern and height were predicted for the same 5415 model at $Fn = 0.28$. Some different surface-capturing methods were applied, giving a dry transom in some cases, a wetted transom in others. In the discussion it was pointed out that the grid density may determine the regime obtained; and that, moreover, the 5415 $Fn = 0.28$ case was rather unsteady in the experiments.

In Wilson et al (2006), results from several methods, for the Athena hull at two Froude numbers, are compared with model-scale data. All methods, mostly belonging to the free-surface capturing RANS/FS category, appeared to give qualitatively good predictions, in particular for a higher-Fn case with smooth flow off the transom. Main deviations were a slight shift of the stern wave crest, and damping of the wave pattern away from the hull. The paper does not address the ability to predict the transition between regimes and other details.

A most detailed recent study on 2D viscous transom flows is Maki et al (2006). They used viscous unsteady free-surface capturing codes, one a level-set code and the other a VOF code, for a flat-bottomed semi-infinite model at a range of transom Froude numbers; and compare with own experimental data. They discern four different flow regimes: a low-speed regime with a wetted transom and little unsteadiness, for $Fn_{tr} < 1$; a subsequent regime with a wetted transom, showing strongly unsteady behaviour in the experiments, extending up to the transition to dry-transom flow; a dry-transom regime having a spilling breaker aft of the transom; and the final dry-transom regime in which the breaking has been shed and a smooth flow occurred, for $Fn_{tr} > 4$ in these experiments. They showed that an indication of the flow regime rather naturally followed from their computations. However, in the computations a much too strong unsteadiness was obtained. It is concluded that the computational tools are not yet ready to give a definitive answer to the problem.

Objectives of this paper

Summarising, it seems that the ability of RANS/FS codes to predict transom flows sometimes seems to be taken for granted, and predictions are simply made without prior study. However, many complicated processes are playing a role, and there are still important questions on the prediction of the flow regime, dealing with wave breaking and its effect on the trailing wave pattern, accomodating transitions between flow regimes in a code, the effect of turbulence modelling and grid density and the effect of the unsteadiness. It is to be noted that, while surface capturing methods may indicate the inception of breaking and survive the overturning of the computed wave surface, the physics playing a role in wave breaking are usually not modelled and not resolved; so for those methods the realism is just as well to be demonstrated.

The present paper then has several objectives. In the first place, we want to check to what extent our RANS code can predict the various flow regimes. It is a surface-fitting method, with a single-valued description of the wave surface; and it is in completely steady form and disregards the unsteadiness. Therefore, success is not guaranteed; but if applicable, this could be a much more pragmatic and efficient approach for ship design purposes than having to carry out a time-accurate simulation of the unsteady phenomena, requiring small time steps and long integration times in order to get a reasonably stable time-averaged result.

Secondly, we want to validate the predictions obtained with available detailed data on transom flows

and the transitions. Thirdly, using the predicted flow fields we want to study and understand the physical characteristics of transom flows, and in particular to study the scale effects occurring, for which there does not seem to be any published information. All this will be addressed in the following sections.

THE RANS SOLVER

The code we use is PARNASSOS (Hoekstra, 1999; Van der Ploeg et al, 2000), which is a RANS solver developed and used by MARIN and IST (Instituto Superior Técnico, Lisbon, Portugal), dedicated to the prediction of the steady viscous flow around ship hulls. It solves the discretised Reynolds-averaged Navier-Stokes equations for a steady, 3D incompressible flow around a ship hull. Of the various turbulence models available we have here used the one-equation model by Menter (1997) and the two-equation k-ω SST model by Menter (1994). The code uses structured multiblock body-fitted grids, usually of HO type.

Central schemes are used for the grid metric and diffusive terms. For the convective terms and in the continuity equation we use second-order upwind schemes in the streamwise direction, and third-order schemes for the normal and girthwise direction. For the gradients of the pressure in the momentum equations we use third-order schemes.

Unlike most other methods, PARNASSOS solves the momentum and continuity equations in their original form, without resorting to e.g. a pressure-correction equation or an artificial-compressibility form. This is enabled by retaining the full coupling of all equations in the solution process. After discretisation and linearisation, the momentum and continuity equations give rise to a matrix equation containing 4*4 blocks, which is solved using GMRES with an incomplete LU-factorisation as a preconditioner. The system of linearised equations is solved, for all variables simultaneously, for subdomains that consist of several streamwise stations at a time. It is possible to choose these subdomains in the range from one plane to even the complete domain. The subdomains are addressed in a downstream sequence. This downstream marching process must be repeated until the solution has converged. More about the solution procedure can be found in (Van der Ploeg, Eça and Hoekstra, 2000).

Free-surface treatment: the steady iterative formulation

The method is of a free-surface fitting type; the upper boundary of the computational domain coincides with (an approximation of) the wave surface all the time, and therefore needs to be updated repeatedly. Free-surface boundary conditions (FSBC's) are imposed here. If we denote the velocity components (in a *(x,y,z)*-co-ordinate system fixed to the ship, with *x* positive aft and *z* upward) by *u,v,w*, the wave height by $\zeta(x,y)$, and non-dimensionalise all quantities using ship speed *U*, a reference length L_{pp}, and gravity acceleration *g*, the free-surface boundary conditions are:

- a kinematic condition,
$$\zeta_t + u\zeta_x + v\zeta_y - w = 0 \quad \text{at} \quad z = \zeta \tag{1}$$
- a normal component of the dynamic condition, requiring that at the surface the pressure is atmospheric ($p=0$); neglecting surface tension and viscous contributions this takes the form
$$Fn^2\psi - \zeta = 0 \quad \text{at} \quad z = \zeta \tag{2}$$
in which $\psi=(p+\rho gz)/(\rho U^2)$ is the non-dimensional hydrodynamic pressure.
- two tangential components of the dynamic condition, requiring that no shear stress is exerted on the water surface.

Almost all other methods for computing viscous free-surface flows solve this problem by following a time-dependent procedure, starting from an initial condition and continuing until a steady result is obtained. As is discussed in (Raven and Starke, 2002), this can lead to a slow formation of the steady wave pattern, persistent time dependence, reflection of waves at artificial boundaries, and contact line problems.

Instead, we use the 'steady iterative' approach, first proposed in (Raven and Van Brummelen, 1999) and derived in more detail in (Van Brummelen et al., 2001). This method avoids all unsteadiness and solves a strictly steady form of the problem directly by iteration. An alternative formulation then is required for solving the nonlinear free-surface problem. This is obtained by substituting the wave elevation from the dynamic condition into the kinematic condition, which yields:

$$Fn^2\left(u\psi_x + v\psi_y + w\psi_z\right) - w = 0 \quad \text{at} \quad z = \zeta\,. \tag{3}$$

This combined condition, together with the three dynamic conditions, gives a set of conditions that corresponds exactly with the original set. In each iteration:

I. the RANS equations are solved subject to the combined condition (3) and the tangential dynamic conditions, imposed at the current wave surface;

II. next, the wave surface and grid are updated using the normal dynamic condition (2).

Upon convergence the pressure deviation, normal velocity and shear stress vanish at the wave surface and the solution of the steady RANS/FS problem has been obtained.

The combined FSBC (3) is easily implemented because we use the fully coupled formulation described above. The derivative of ψ in main stream direction must be modelled by an upwind-biased difference scheme. We use a third-order 4-point scheme, except in the first stations behind the transom, where lower-order upwind schemes must be used.

Several applications (Raven and Starke 2002), (Raven et al, 2004), (Hino, 2005) have shown that the steady iterative formulation not only is very efficient, often requiring an order of magnitude less CPU time, but, with the discretisation schemes used, also provides accurate results with very low numerical wave damping. In (Raven et al, 2004) a theoretical analysis of the numerical dispersion and damping is carried out, indicating that we have a third-order numerical damping and third-order numerical dispersion, explaining the good properties.

In the present study, the transom flow regime has been preselected and then the limits of that regime have been determined. For a dry-transom flow, the pressure at the transom edge is set equal to the atmospheric pressure. For a wetted transom, no special condition at the transom edge is imposed; on the transom, no-slip conditions are imposed, and the wall-normal derivative of the pressure is zero. Hence the level of the free surface is not fixed in this case.

For the present applications, one further adjustment was required. Especially at full-scale an extreme clustering of nodes towards the hull is needed. Because we use a structured grid, we also have extremely small mesh spacing normal to the free surface in the present test cases. If the diffusive terms are treated implicitly, their contributions in the coefficient matrix completely dominate those from the convective terms and the pressure gradient. This more or less decouples the pressure at the free surface from that below the free surface, preventing convergence. Therefore, the diffusive terms in the fourth boundary condition here are implemented explicitly i.e. they are taken from the previous inner iteration. With this adaptation, the convergence behavior strongly improves.

THE COMPUTATIONAL MODEL

Using a steady free-surface fitting technique, we were aware of the possible limitations in predicting the various transom flow regimes, including the effects of unsteadiness and wave breaking. The question then was: how can we identify the proper transom flow regime, for a given ship and speed? The answer is sought by approaching the transition between flow regimes from both sides: starting from a dry transom condition, and systematically increasing the transom draught; and starting from a wetted transom and decreasing it.

The computational model can be described as a backward-facing step with free surface, see Fig. 1. It consists of a flat-bottomed plate with a length of L_{pp} = 100 m. and a prescribed transom draught for each computation, typically varying between T_{tr} = 0.1 and T_{tr} = 0.5 m. in the case of dry-transom conditions, and between T_{tr} = 0.45 and T_{tr} = 1.5 m. in the case of wetted transom conditions. The origin of the co-ordinate system was located at the intersection of the transom with the still-water level.

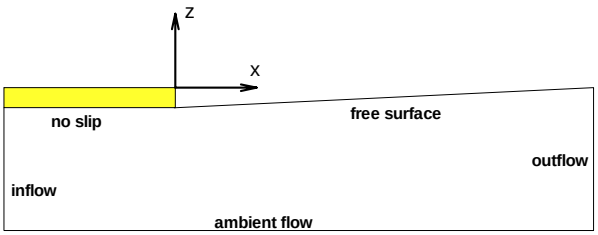

Figure 1: A sketch of the computational domain and the applied boundary conditions.

The inflow boundary was located halfway the plate, with an estimated boundary-layer profile for the mean velocities and the turbulence quantities. Downstream, the outflow boundary was located $1L_{pp}$ behind the transom. In vertical direction the computational domain extended $0.15L_{pp}$ from the undisturbed free surface. Note that these last two boundaries should be chosen sufficiently far from the plate not to influence the solution. Along the width of the plate a limited number of cells was used with symmetry boundary conditions imposed on the corresponding faces of the mesh, because we have used our 3D RANS solver to compute this two-dimensional flow problem.

Unless mentioned otherwise, the computations have been performed both at model scale and at full-scale Reynolds number, with a flow speed of V_s = 10 knots and a scale factor of 20. This results in the following parameters for the Froude number and the Reynolds numbers, based on the length of the plate:

Fn = 0.164,
Rn = 4.5 x 10^8 (ship), 5.1 x 10^6 (model).

In potential-flow theory the present computational model consists of a plate that stretches infinitely far upstream. In that case the Froude number based on the length of the plate is of no use, and the transom draught is the only length scale present in the model and thus the main parameter determining the flow. In the present study the Froude number based on the transom draught

runs between Fn_{tr} = 1.34 for a transom immersion of 1.5 *m*. to Fn_{tr} = 5.19 for a transom immersion of 0.1 *m*.

RESULTS FOR THE DRY TRANSOM

In the computations presented in this section the pressure at the transom edge has been set equal to the atmospheric pressure so that the transom is, by definition, not wetted. The aim of the computations is to study the flow behaviour with increasing transom immersion. It can be expected that the amplitude of the trailing wave system increases with increasing transom draught. At the same time the flow velocity in the top of the waves can be expected to decrease. By the time the flow stagnates in the top of the first wave crest, wave breaking will have occurred in reality. As wave breaking is not modelled in the present computations, an important aspect of the investigation is the behaviour of our flow solver and the predicted flow fields and wave elevations approaching this flow regime.

Computations have been performed on a single-block, structured mesh with in the

coarsest mesh: (26 + 126) x 20 cells,
medium mesh: (52 + 252) x 30 cells,
finest mesh: (104 + 504) x 40 cells

in the streamwise and the vertical direction, respectively. The two numbers for the streamwise direction correspond to the number of cells on the plate and in the wake, respectively. Both on the plate and in the wake cells are clustered towards the transom. Furthermore grid cells are clustered in vertical direction towards the plate, to capture the gradients that occur in the boundary layer. The non-dimensional wall distance y^+_{max} < 0.40 for all viscous-flow computations. Menter's one-equation model has been used to model the effect of turbulence on the mean flow.

The initial shape of the wave surface in each computation was simply estimated to be a straight line between the edge of the transom and the still-water level at the outflow boundary. Then the RANS equations are solved, followed by a free-surface update. Upon convergence, the solution of the steady RANS/FS problem has been obtained. Figure 2 shows the convergence histories of the free-surface updates for three transom immersions that are representative for the computations presented in this section. For the smallest immersion considered (T_{tr} = 0.10 *m*.) the convergence is fast; after only five updates the maximum change in the wave elevation between two updates has dropped below $dz/L_{pp} = 10^{-6}$. However, the convergence speed is found to decrease with increasing immersion, and for the most challenging case considered (T_{tr} = 0.516 *m*.) approximately ninety free-surface updates were required to reach the same convergence level. It will be shown in the second half of this section that for this last case the flow almost stagnates in the top of the first wave crest.

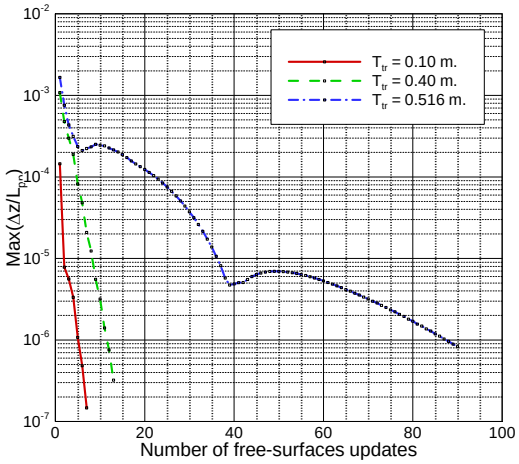

Figure 2: The convergence history of the free-surface updates on the finest mesh for three transom immersions. Inviscid-flow computations.

Inviscid-flow computations

Accurate nonlinear potential-flow solutions for the present test case have been obtained by Vanden-Broeck (1980). He provides the wave profile behind the transom for a transom-Froude number of Fn_{tr} = 2.35, as well as the steepness of the waves for a range of transom-Froude numbers. Using our viscous-flow solver, effectively inviscid solutions of the present problem were obtained by changing the no-slip condition on the wall to free slip and by imposing a homogeneous velocity field at the inflow boundary.

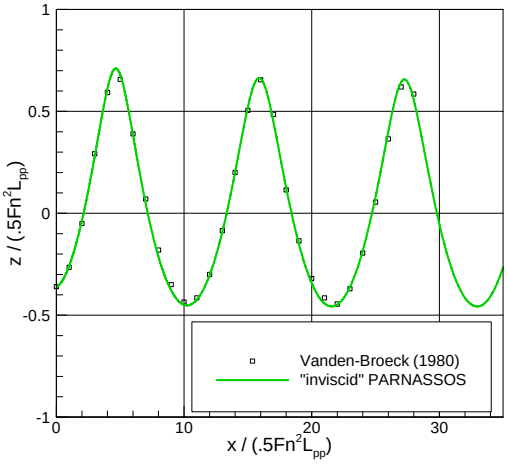

Figure 3: Comparison between the wave heights predicted by nonlinear potential-flow (symbols) and the present inviscid-flow solution (solid line).

In Fig. 3 excellent agreement is shown at this transom-Froude number between the predicted free-surface elevation according to the nonlinear potential-flow solution by Vanden-Broeck and the present inviscid solution.

Also at other transom-Froude numbers excellent agreement is obtained between the two methods. This is illustrated in Fig. 4, showing the variation of the wave steepness, *s*, with the transom-Froude number. Here the wave steepness is defined as the ratio between the wave amplitude (the difference between a wave crest and a wave trough) and the wave length.

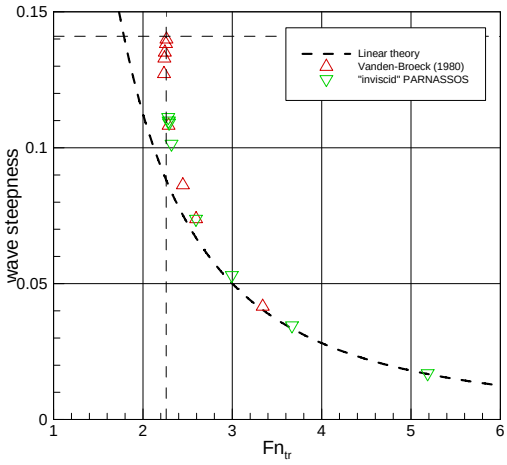

Figure 4: The relation between the wave steepness and the transom-Froude number for inviscid flow.

The two straight dashed lines in this figure indicate the limiting case reported by Vanden-Broeck, where a wave steepness of s = 0.141 is reached at a transom-Froude number of 2.26. Below Fn_{tr} = 2.23 no inviscid flow solutions can exist without wave breaking. The curved dashed line corresponds to linear wave theory, according to which the wave steepness would grow unboundedly with decreasing transom-Froude number. Both the nonlinear solution and the present inviscid solution agree very well with the linear theory for $Fn_{tr} > 3$. At lower transom-Froude numbers these solutions start to deviate from the linear solution, and the wave steepness is found to increase rapidly towards the limiting value as the value of Fn_{tr} = 2.26 is approached.

The good agreement between the nonlinear potential-flow solution and the present inviscid solution illustrates the accuracy that can be obtained with our free-surface method; and provides an accurate starting point for the following investigation of viscous effects.

Figure 5 presents an example of the variation of the pressure coefficient along the aft end of the plate and the free surface. At the aft end of the plate the pressure shows an approximate square-root behaviour in accordance with the theory pointed out by Schmidt (1981). Further downstream the pressure increases and decreases in phase with the following wave crests and wave troughs. The corresponding wave elevation follows from the pressure distribution along the free surface using the normal component of the dynamic FSBC.

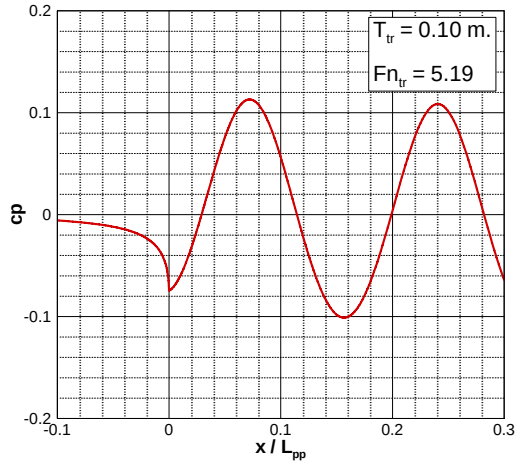

Figure 5: The pressure distribution along the aft part of the plate and along the free surface in the near wake.

In the top part of Fig. 6 wave patterns are shown for the three cases of which the convergence histories were already shown in Fig. 2. Following Maki (2006) the wave height has been non-dimensionalized with the transom immersion of each case, and the streamwise co-ordinate with the linear wave length, defined as

$$\lambda_{lin} / L_{pp} = 2\pi Fn^2 = 0.169$$

As expected the wave height increases with increasing transom immersion, but the height of the first wave crest aft of the transom grows faster than the following wave crests due to the near-field disturbance. At the same time the length of the trailing wave system is reduced due to nonlinear effects. Nonlinear effects also cause the wave crests to become sharper and the wave troughs to become broader. The reduction of the wave lengths is quantified in Table 1. There it can be seen that for the smallest transom immersion considered the wave length is practically equal to the linear wave length. For a transom-Froude number of Fn_{tr} = 2.59 the wave length is reduced to approximately 95 per cent of the linear wave length, and for the smallest transom-Froude number considered, Fn_{tr} = 2.28, it is reduced to 88 per cent of the linear wave length.

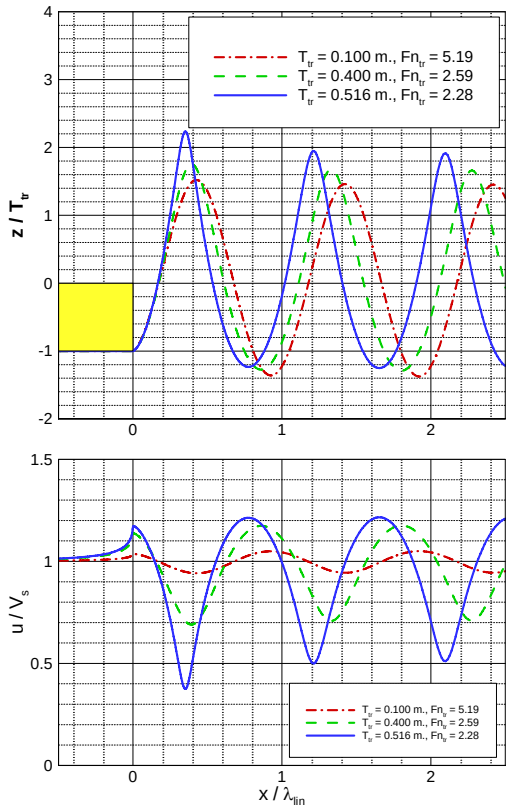

Figure 6: The wave profiles (top) and the axial velocity along the free surface (bottom) for various transom immersions. Inviscid-flow computations.

Related to the increase of the wave height with increasing transom immersion is a decrease of the velocity along the free surface. This is illustrated in the bottom part of Fig. 6. Here it can be seen that the axial velocity along the free surface has alternatingly minimum and maximum values in the wave crests and the wave troughs, respectively. The axial velocity in the top of the first wave crest aft of the transom is found to decrease fast for decreasing transom-Froude numbers, especially close to the limiting value. As mentioned before, according to the nonlinear theory by Vanden-Broeck the velocity in the top of the first wave crest should vanish for $Fn_{tr} = 2.26$, which is only marginally smaller than the smallest transom-Froude number shown in Fig. 6. In the present inviscid-flow computations we were not able to obtain sufficiently converged free-surface elevations for $Fn_{tr} < 2.28$. Note, however, that at this transom-Froude number the minimum value of the axial velocity in the top of the first wave crest is still equal to $u/V_s = 0.38$. Therefore it can be concluded that only a small further increase of the transom immersion (25 *mm*. in the present test case) will result in a relatively strong reduction of the velocity in the top of the first wave crest, causing the flow to stagnate.

Table 1: Distance between successive wave crests, expressed as a fraction of the linear wave length.

	$2^{nd} - 3^{rd}$	$3^{rd} - 4^{th}$	$4^{th} - 5^{th}$
$T_{tr} = 0.10$ *m.*, $Fn_{tr} = 5.19$	0.99	0.99	1.00
$T_{tr} = 0.40$ *m.*, $Fn_{tr} = 2.59$	0.94	0.95	0.94
$T_{tr} = 0.516$ *m.*, $Fn_{tr} = 2.28$	0.89	0.88	0.88

Viscous-flow computations

Similar to the inviscid-flow computations presented in the previous subsection, viscous-flow computations were carried out for the present test case. The main difference between the two flows is the presence of a boundary layer on the no-slip wall in the viscous-flow computations. Compared to the inviscid flow the boundary layer introduces a velocity deficit in the neighbourhood of the edge of the transom, which will affect the wave generation. Again, the transom immersion has been systematically increased, starting from $T_{tr} = 0.10$ *m.*, until the flow practically stagnated in the top of the first wave crest.

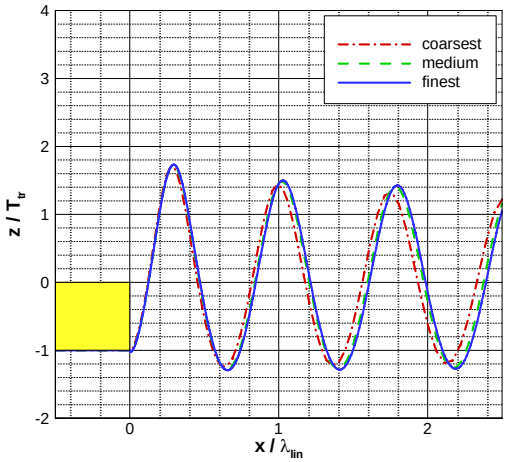

Figure 7: The mesh dependence of the wave elevation at model scale Reynolds number. $Fn_{tr} = 5.19$.

An indication of the mesh dependence of the viscous-flow solutions presented in this section is given in Fig. 7. There the predicted free-surface elevation at model scale for the case $Fn_{tr} = 5.19$ is given for the coarsest, medium and finest mesh. The figure shows an increase of both the predicted wave length (numerical dispersion) and the predicted wave amplitude (numerical damping) with increasing mesh density. The

solution at the coarsest mesh is apparently not accurate enough, but the solutions on the medium and the finest mesh practically coincide on the scale shown. It has been verified that the increase in the maximum wave height is approximately 7 per cent between the coarsest and the medium mesh, and 1 per cent between the medium and the finest mesh. While the distance between the transom and the third wave crest increases with 2.7 per cent of the linear wave length between the coarsest and the medium mesh, and with only 0.7 per cent between the medium and the finest mesh. It was therefore concluded that the solutions at the finest mesh are sufficiently accurate for the present purposes, and in the following only solutions obtained at the finest meshes will be used.

In the top part of Fig. 8 and Fig. 9 wave profiles are shown for model scale and full scale, respectively. The solutions correspond to three cases from our systematic variation, namely the one with the smallest transom immersion studied here, the one where the flow almost stagnates in the top of the first wave crest and one with a transom immersion in between these two. The global impression of the variation of the wave pattern with the transom immersion is similar to what was found for inviscid flow, namely, with increasing immersion the wave amplitudes increase, especially that of the first wave which grows to more than twice the height of the transom immersion. At the same time the wave length is reduced. However, there are some striking differences as well. First of all the reduction of the wave length due to nonlinear effects is much stronger in the viscous flow fields than in the inviscid flow field, and more so at model scale than at full scale. This is further quantified in Table 2. There the distance between successive wave crests is listed for the case with the smallest transom immersion, $T_{tr} = 0.10\ m$. As reported in the previous subsection, the wave length in inviscid flow is practically equal to the linear wave length for this case. For viscous flow the distance between the second and third wave crest in the solution has been reduced to 87 per cent of the linear wave length at full scale, and to 77 per cent of the linear wave length at model scale.

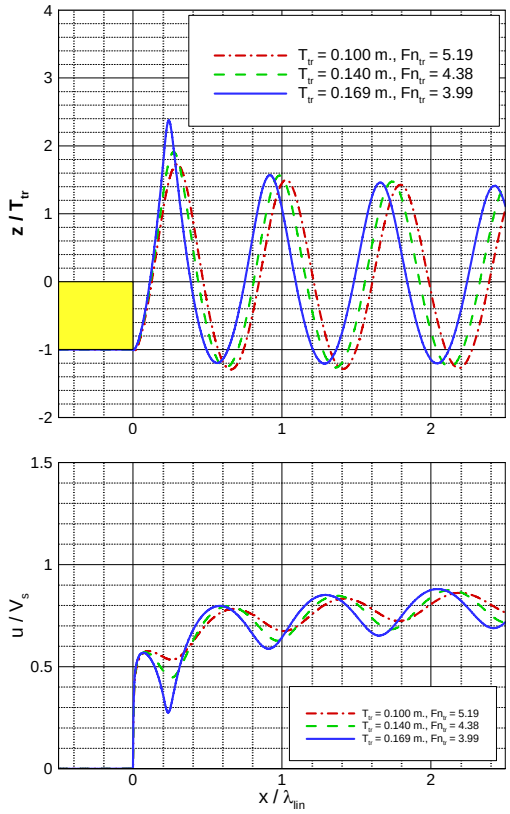

Figure 8: The wave profiles (top) and the axial velocity along the free surface (bottom) for various transom immersions at model-scale Reynolds numbers.

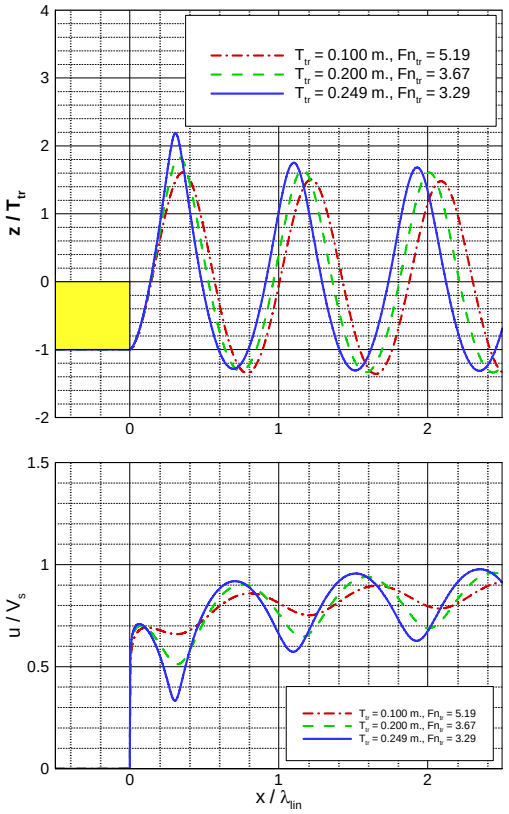

Figure 9: The wave profiles (top) and the axial velocity along the free surface (bottom) for various transom immersions at full-scale Reynolds numbers.

Furthermore it can be seen that, whereas the wave length remains constant with streamwise direction in the inviscid flow, the wave length in the viscous flows shows a gradual increase in downstream direction. This is caused by the acceleration of the viscous flow aft of the transom, causing a change of the propagation speed for steady waves.

It can also be seen from Fig. 6, Fig. 8 and Fig. 9 that the transom immersion at which the highest waves occur is significantly smaller at full scale, compared to the inviscid flow, and significantly smaller at model scale, compared to full scale. This will be discussed in more detail in the next subsection.

Table 2: The distance between successive wave crests, expressed as a fraction of the linear wave length.

$T_{tr} = 0.10\ m.$, $Fn_{tr} = 5.19$	$2^{nd} - 3^{rd}$	$3^{rd} - 4^{th}$	$4^{th} - 5^{th}$
Inviscid	0.99	0.99	1.00
Ship	0.87	0.89	0.89
Model	0.77	0.79	0.81

To illustrate the observed scale effect on the wave length more clearly, Fig. 10 presents the three solutions for the case $T_{tr} = 0.10\ m.$, $Fn_{tr} = 5.19$ in a single graph. Visible in the top part of this figure is the phase shift and the reduction in wave length between the inviscid flow and the two viscous-flow solutions. Directly aft of the transom the lower velocities in the inner parts of the boundary layer at model scale result in a smaller radius of curvature of the free surface, compared to full scale and the inviscid flow. Consequently at model scale the forward face of the wave is steeper, thus introducting the phase shift. Obviously, further downstream the phase difference is also affected by the observed difference in wave length between the three flows.

In the bottom half of Fig. 10 the axial velocity along the free surface is shown for the same case. As could be expected, the axial velocity oscillates around $u/V_s = 1$ in the inviscid-flow solution. In the viscous flow, due to the no-slip boundary condition on the surface of the plate, the flow velocity is equal to zero at the transom and then accelerates to the free-stream velocity (infinitely) far downstream. The acceleration of the flow is alternatingly reduced and increased in phase with the successive wave crests and wave troughs, respectively. As a reference, also shown in the bottom half of Fig. 10 is the acceleration of the flow in the wake of an infinitely thin flat plate subject to zero pressure gradient. In that computation symmetry boundary conditions have been imposed at the flat water surface in the wake of the plate. Comparing the two solutions it can be seen that the "average" increase of the axial velocity in the present test case is in close agreement with the acceleration of the flow in the wake of the flat plate.

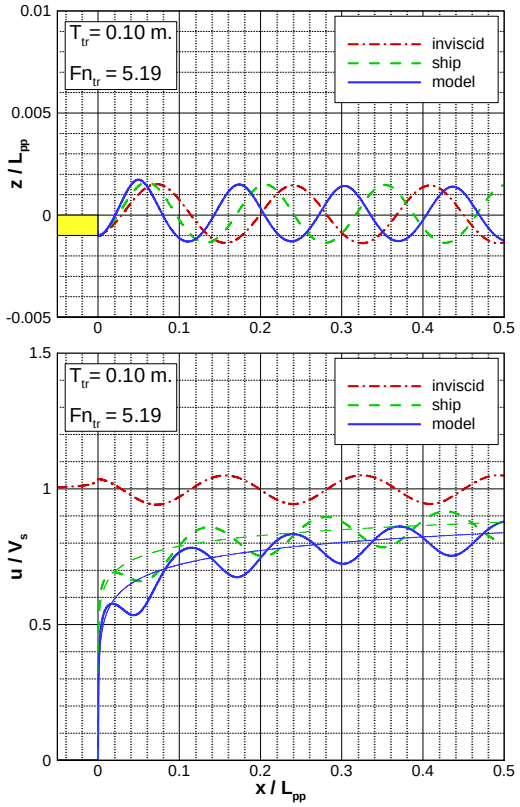

Figure 10: The scale effect on the wave elevation (top) and the axial velocity along the free surface (bottom). The thin lines in the bottom half of the figure correspond to the acceleration of the flow in the wake of a flat plate at zero pressure gradient.

Scale effect on inception of stern wave breaking

Furthermore it is evident from Fig. 10 that there exists a large scale effect on the velocity field, just as on the wave pattern. This can most clearly be demonstrated by comparing the minimum velocities in the top of the first wave crest of each of the three flows. In the inviscid flow solution the magnitude of the axial velocity is locally equal to $u/V_s = 0.94$, while it is reduced to $u/V_s = 0.66$ and $u/V_s = 0.53$ for the full scale and the model scale solutions, respectively. This reduction is a consequence of the momentum loss in the boundary layer, which also makes that the flow is less able to overcome the hydrodynamic pressure rise towards the top of the first wave crest. While, on top of that, the steepness of the initial wave aft of the transom was found to increase with decreasing Reynolds number. Thus it can be understood that with increasing transom immersion the flow will stagnate sooner (that

is, at smaller transom immersions) in the top of the first wave crest at model scale, compared to full scale and inviscid flow. While in the absence of a wake at the wave surface breaking occurs when the limiting inviscid wave steepness is approached (e.g. Duncan 1983), the wake leads to wave breaking at a much lower steepness and, in this case, transom immersion.

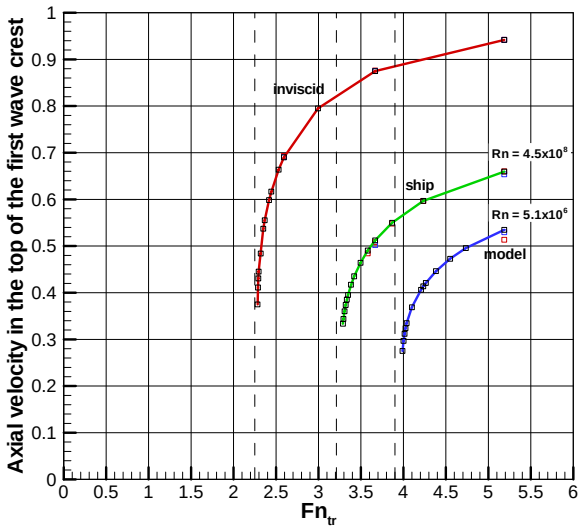

Figure 11: Variation of the axial velocity in the top of the first wave crest with the transom-Froude number.

In that respect Fig. 11 presents arguably the most important result of the present section. Shown is the velocity in the top of the first wave crest against the transom-Froude number for all the cases in our systematic variation of the transom immersion; and both for the inviscid flow and for the viscous flow at model and full scale Reynolds number. All three solutions show an asymptotic behaviour of the velocity in the top of the first wave crest with decreasing transom-Froude numbers. But stagnation of the flow in the top of the first wave is found to occur at a considerably higher transom-Froude number (smaller transom immersion) at model scale than at full scale and in inviscid flow. For the inviscid flow stagnation is found to occur at Fn_{tr} = 2.26, which is in excellent agreement with the nonlinear potential flow theory discussed in the first part of this section. This transom-Froude number corresponds to a transom immersion of T_{tr} = 0.516 *m*. in the present test case. At full scale Reynolds number stagnation is predicted at a higher transom-Froude number of Fn_{tr} = 3.29, corresponding to a transom immersion of T_{tr} = 0.249 *m*. At model scale, finally, stagnation occurs at a transom-Froude number of Fn_{tr} = 3.99, corresponding to a transom immersion of T_{tr} = 0.169 *m*. This last result is in good agreement with the experimental observation by Maki (2006), who stated that "based on general observations on the experimental set-up wave breaking is shed aft of the first wave crest near a transom-Froude number of Fn_{tr} = 4, leaving an attached, steady, gravity wave". We suppose here that a vanishing of the velocity component along the wave surface is an adequate indication of the inception of wave breaking. As a matter of fact, this criterion has been found to be valid in experiments, and has a more universal validity than criteria based on wave slope or free-surface curvature (which do not take into account the effect of a wake or surface current) or vertical acceleration.

An important consequence of these results is that there is a range of transom-Froude numbers ($3.29 < Fn_{tr} < 3.99$ for the present test case) where a spilling breaker occurs in the flow at model scale, while there is a smooth flow without any wave breaking at full scale. The extent of this range, i.e. the magnitude of the scale effect on the inception of breaking, might be surprising: the onset of stern wave breaking at full scale occurs only at a transom immersion almost 1.5 times larger than at model scale; and this is only caused by the difference in the boundary layer and wake from the bottom of the vessel.

In order to get some understanding of the strength of this effect, we compare with a very simple theory proposed by Banner & Phillips (1974), for the equally remarkable effect of wind drift on incipient breaking of wind waves. Wind drift is considered as a thin surface layer in which the velocity differs from the wave orbital velocity beneath, and which responds to the surface straining in the wave motion; somewhat similar to the vessel's wake along the surface responding to the retardation towards the wave crest. They indicate that the maximum height the waves can attain without breaking is the height at which the combined surface velocity vanishes. This height is approximately proportional to $(1-\gamma)^2$, where γ is the ratio of mean surface drift velocity to wave speed. Substituting there the velocity deficit in the wake at the location of the first crest, disregarding the wavy variations, from figures similar to Fig. 8 but for larger transom immersion, we get about γ = 0.4 at model scale, γ = 0.3 at full scale. The maximum wave height without breaking thus would be 36% and 49% of the inviscid limiting wave height for model and full scale, respectively. The largest values achieved in our computations are 30% and 41%, respectively. While there are many differences and approximations, at least this simple theory lends some support to the unexpected magnitude of the boundary layer effect on the wave breaking aft of the transom.

RESULTS FOR THE INTERMEDIATE REGIME

For transom-Froude numbers between the critical values that were determined for the dry-transom regime

in the previous section and that will be determined for the wetted-flow regime in the following section, the flow smoothly separates from the transom, but has a spilling breaker on the forward face of the first wave. A priori it is not evident that solutions can be obtained in this range with a steady, surface-fitting method without any wave-breaking model. And indeed we experienced a deterioration of the convergence speed of the free-surface updates when approaching this intermediate regime, as illustrated in Fig. 2. However, until now we did manage to obtain converged results for a few cases, one of which is shown in Fig. 12. For a transom-Froude number of Fn_{tr} = 2.77 the flow is found to separate smoothly from the transom. Almost immediately aft of the transom a steep rise in the wave elevation is found, with an area of flow reversal in the top of it. Further downstream the water level slowly rises to the top of the first wave crest. During the computations we observed that the exact location of the forward face of the wave is fairly ill-determined, as it tended to shift slowly upstream with each free-surface update, until convergence. We like to stress that we do not expect that the location of the forward face has been determined accurately in this particular computation. First of all only two grid cells are located on the forward face of the breaker in the present mesh, and therefore further grid refinement is necessary to investigate the sensitivity of its location to the discretization error. Secondly, the lack of a wave breaking model is bound to have an effect on the solution. Nevertheless we think it is striking that physically acceptable results can be obtained for this test case with a steady, surface-fitting approach in this flow regime.

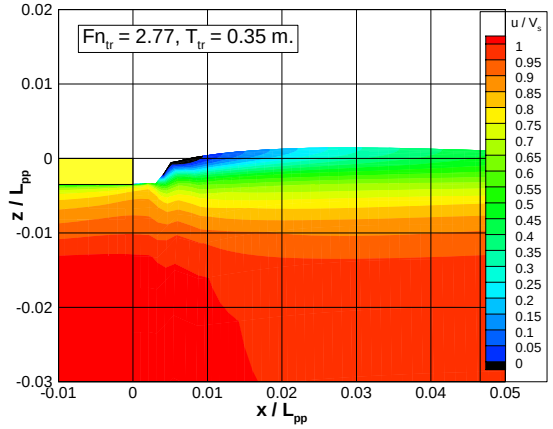

Figure 12: An example of the predicted flow field at model scale in the intermediate regime.

RESULTS FOR THE WETTED TRANSOM

In a preceeding section results of a systematic variation of the transom flow have been presented starting from the dry-transom regime (high transom-Froude numbers) and going towards the regime were wave breaking is known to occur. In the present section we approach this region from the opposite direction, namely from the region where the transom is -partially-wetted and we systematically increase the transom-Froude number, until the water reaches the edge of the transom.

The computational domain and grid lay-out is practically identical to the one presented in Fig. 1, with the sole exception that grid cells are now distributed over the wetted part of the transom as well. A detail of the mesh for wetted-transom flow is shown in Fig. 13.

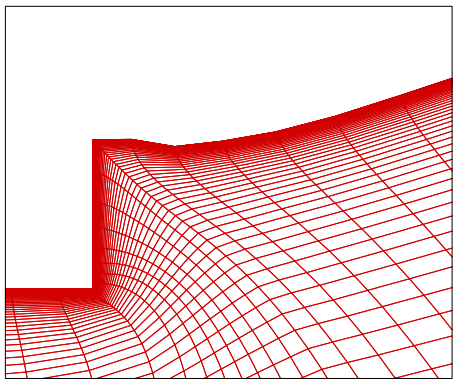

Figure 13: A detail of the computational mesh near the transom for the wetted flow regime.

Computations have been performed on a single-block structured mesh with in the

coarsest mesh: (20+ 5+ 95) x 80 cells,
medium mesh: (52+ 9+189) x 100 cells,
finest mesh: (104+17+377) x 120 cells

in the streamwise and the vertical direction, respectively. The numbers for the streamwise direction correspond to the number of cells on the plate, on the wetted part of the transom and in the wake, respectively. Both on the plate and in the wake cells are clustered towards the transom. Furthermore cells are clustered in vertical direction towards the plate, to capture the gradients that occur in the boundary layer. The non-dimensional wall distance $y^+_{max} < 0.40$ for all viscous flow computations. The k-ω SST model by Menter (1994) has been used to model the effect of turbulence on the mean flow.

The initial shape of the wave surface in each computation was estimated to coincide with the still-water level. Then the RANS equations were solved, followed by a free-surface update. In the free-surface updates the water level was free to move up and down the transom. Upon convergence, the solution of the steady RANS/FS problem has been obtained. Figure 14 shows the convergence history for a case where the transom-Froude number is equal to Fn_{tr} = 2.23. Convergence is fast, and in ten free-surface updates the maximum changes in the free-surface elevation between two successive iterations have dropped below $dz/L_{pp} = 10^{-6}$.

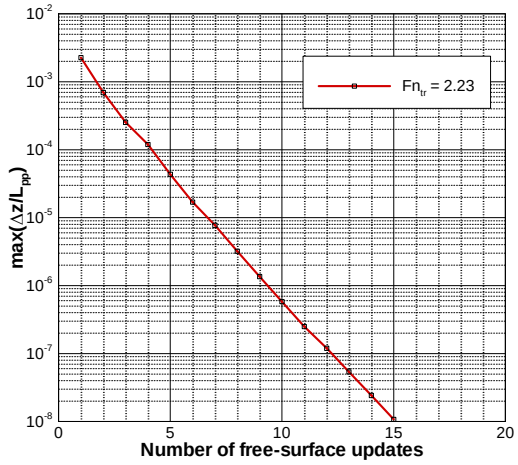

Figure 14: The convergence history of the free-surface updates for one of the cases in the wetted-flow regime.

For the present test case experimental data are available from Maki (2006) at model scale Reynolds number. We have compared our computational results with his measurements at the following two conditions,

Fn_{tr} = 1.92, Fn = 0.196, Rn = 1.3 x 10^6, and
Fn_{tr} = 2.23, Fn = 0.210, Rn = 1.4 x 10^6.

Note, that these parameters are different from the ones used in the systematic variations of the transom immersion presented in other sections of this paper.

Fig. 15 compares the measured and the predicted wave elevation aft of the transom for these two conditions. In both cases the height at which the flow separates from the transom is over-predicted by less than 7 per cent of the transom immersion, using the k-ω SST turbulence model. It is found that both the slope of the first wave and the height of the first wave crest are somewhat under-predicted. As a result the location of the top of the first wave crest lies further aft in both computations. Further downstream the amplitude of the trailing wave systems appears to be captured fairly well. Despite the differences we consider the agreement between the computations and the experiments to be very acceptable. Especially considering that the experimental flow was reported to be strongly unsteady, with maximum r.m.s.-values of the free-surface elevation of 15 to 20 per cent of the transom immersion at the present conditions, while steady-state solutions were obtained in the computations.

To investigate the influence of the turbulence model for this test case, the flow at Fn_{tr} = 2.23 has also been computed using Menter's one-equation model. This model is relatively unknown but has been extensively used at MARIN in recent years for wake-field predictions. It is found that the difference in the predicted wave elevation with the two turbulence models is of the same order of magnitude as the difference between the computed results and the experiments. The choice of the turbulence model has therefore only a limited effect on the accuracy of the predictions. The only exception is the predicted water height at the transom, which is over-predicted by 15 per cent of the transom immersion for the present condition using the one-equation turbulence model.

With respect to the influence of the mesh density on the solutions, it was found that the predicted wave elevations obtained at the medium and the finest meshes practically coincide at the scale shown in Fig. 15. In the following therefore only results obtained at the finest meshes will be used.

Figure 16 presents a global view of the velocity field for these two cases. Clearly visible is the reduction of the wave height directly aft of the transom, followed by an increase of the wave elevation towards the first wave crest. Beneath this part of the wave surface a recirculation area is found, which decreases in length with increasing transom-Froude number, simultaneously with the reduction of the wetted part of the transom. The size of the recirculation area is indicated by streamlines that approximately connect the bottom edge of the transom with the location at the free surface where the axial velocity changes sign. Expressed in terms of the transom draught of each case, the length of the recirculation area changes from 2.77T_{tr} for the case where Fn_{tr} = 1.92 to 2.65T_{tr} for the case where Fn_{tr} = 2.23.

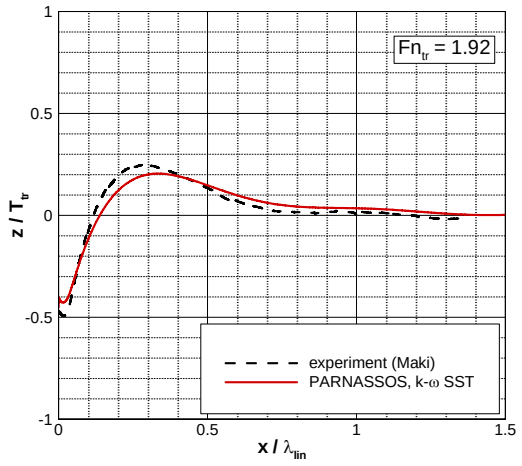

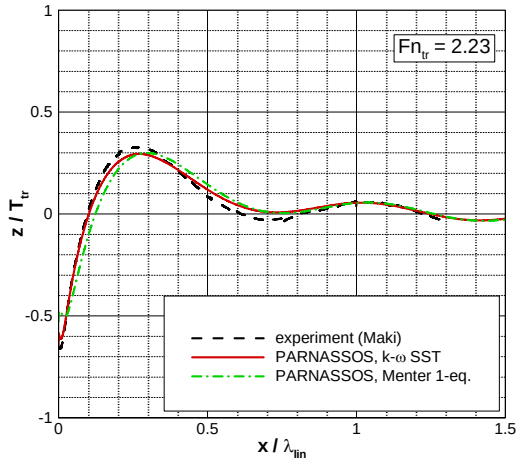

Figure 15: Validation of the predicted wave elevation in wetted-transom flow at two transom-Froude numbers.

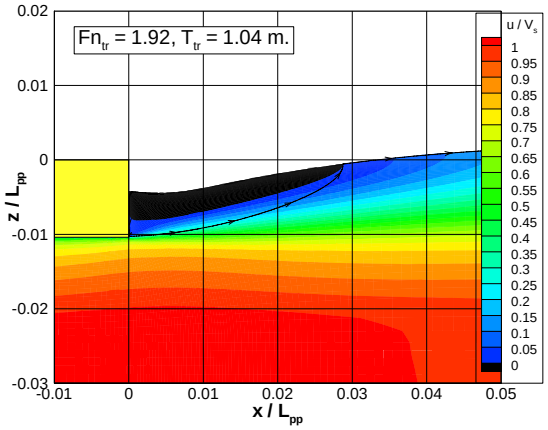

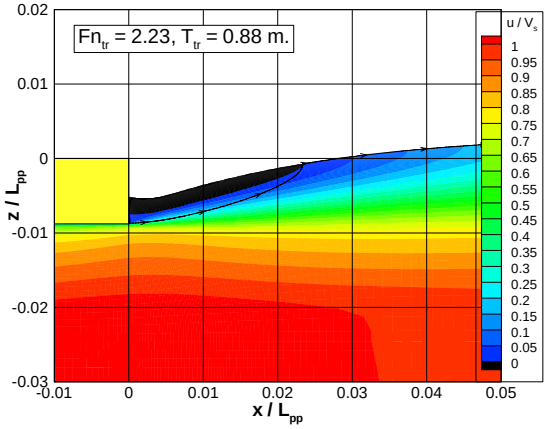

Figure 16: The flow field aft of the wetted transom for the same conditions as shown in Fig. 15.

A systematic study of the clearing of the transom has been performed for the same Froude number and Reynolds numbers based on the length of the plate as in the section where the dry-transom regime was studied, namely

$Fn = 0.164$,
$Rn = 4.5 \times 10^8$ (ship), $Rn = 5.1 \times 10^6$ (model).

Computations have been performed both at model scale and at full scale Reynolds number starting with a transom immersion of $T_{tr} = 1.5\ m$. ($Fn_{tr} = 1.34$) which was systematically reduced until the transom was almost entirely cleared. Figure 17 presents the transom clearing as a function of the transom-Froude number. At both Reynolds numbers the clearing of the transom varies smoothly with increasing Fn_{tr}. At model scale the present computations indicate total ventilation of the transom near $Fn_{tr} = 2.5$. This is in excellent agreement with the experiments of Maki, who reports the same value of the critical Froude number as the point where the transom first entirely ventilates.

Along the entire range of transom-Froude numbers it is found that ventilation is larger at full scale than at model scale for the same transom immersion. For instance at $Fn_{tr} = 2$, the transom is ventilated for 44 per cent at model scale, compared to 66 per cent at full scale. Consequently the transom ventilates at a lower transom-Froude number (a little higher than $Fn_{tr} = 2$), at full scale compared to model scale. As a result there is a range of transom-Froude numbers where the transom is just cleared at full scale, with a spilling breaker downstream, while the flow is still attached to the transom at model scale. For the present test case

this occurs for transom immersions roughly in the range 0.43 $m. < T_{tr} < 0.67\ m.$

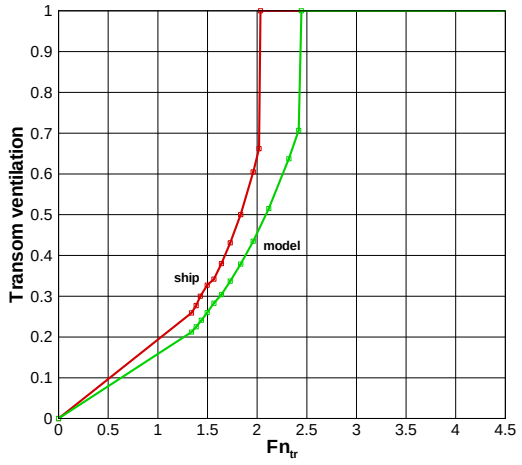

Figure 17: The scale effect on the ventilation process of the wetted transom.

TRANSOM RESISTANCE

The drag of the semi-infinite flat-bottomed body consists of frictional drag on the horizontal bottom surface, plus pressure forces acting on the transom. For the body at rest, hydrostatic pressure would act on the transom, giving a negative resistance contribution at zero speed, which is not cancelled by an equal and opposite force on a forebody for this sem-infinite vessel. So to get a physically meaningful transom resistance, we must subtract this zero-speed hydrostatic force on the transom from the result. Thus, we define the transom pressure resistance coefficient *Ctr* for the object considered as the sum of two contributions:

- the change of the integral of hydrostatic pressure over the transom, relative to the zero-speed case,

$$Cstat = \frac{(\varsigma / L)^2}{Fn^2}$$

- the hydrodynamic pressure integrated over the wetted area of the transom,

$$Cdyn = -\int_{z=ztr}^{\varsigma} c_{pdyn}.d(\frac{z}{L})$$

For a dry-transom flow, the last contribution vanishes, and the transom resistance is simply $C_{tr} = \frac{(z_{tr} / L)^2}{Fn^2}$. This applies from the moment of full unwetting, i.e. also to cases with a spilling breaker aft of the transom.

It should be noted that for other bodies, with sloping buttocks towards the transom, there may be additional resistance contributions associated with a change of the pressure field upstream of the transom.

The two transom resistance contributions have been determined separately for the wetted-transom computations, for model and full scale. Fig. 18 shows how with decreasing draft (increasing Fn_{tr}) the hydrodynamic part decreases quickly, and vanishes when the transom is fully cleared; while the hydrostatic contribution is essentially constant. We have added a line for the total resistance in the dry-transom regime. We observe:

- that the transom resistance in the wetted regime is less than it would be for a dry transom with equal immersion, at least for this particular case;
- that the total transom resistance is somewhat larger for full scale than for model scale, in the wetted regime;
- that this scale effect is present only in the wetted regime, while for a dry transom the same value is valid for inviscid, model and full scale alike.

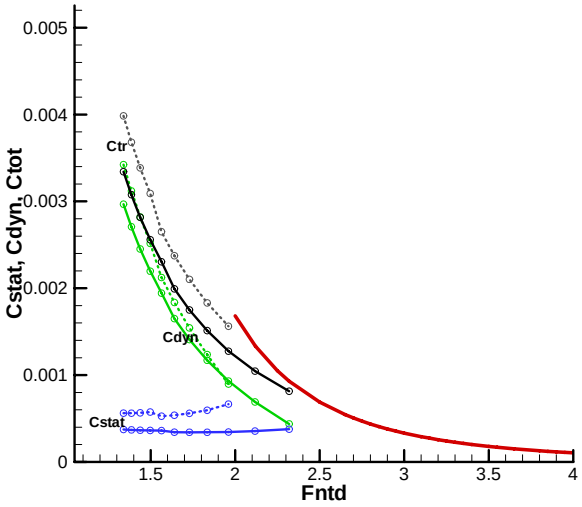

Figure 18: Transom resistance components from RANS computations. Blue: *Cstat*; Green: *Cdyn*; black: *Ctr*. Dashed lines are for full scale, full lines for model scale. The red line at the right is the dry-transom total resistance.

In a detailed inspection of the results, it was observed that for much of the wetted-transom regime, the wave elevation on the transom was nearly constant regardless of the transom draft; as is also observed from the behaviour of *Cstat* in Fig.18. This suggests a very simple analysis, which provides a basic understanding of the principal mechanism of the transom unwetting and the associated resistance, as follows.

- Consider the transom stern resistance as a 'base drag' as occurs on aerodynamic shapes with cut-off trailing ends. This base drag is caused by a reduction of the hydrodynamic pressure on the base, caused by the 'jet-pump' effect of the

surrounding flow that exerts an entraining force on the recirculation region aft of the base.

- Since the velocities in the recirculation region are rather small, we assume that the pressure is essentially constant here, $cp = cp_{base}$ Therefore, $Cdyn = cp_{base}.(z_{Tr} - \varsigma)$
- The waterline height on the transom is related with the base pressure by :

$$\zeta / L = \frac{1}{2} Fn^2 Cp_{base} \qquad (4)$$

yielding $C_{stat} = \frac{1}{4} Fn^2 Cp_{base}^2$

- Consistent with the model is the assumption that the transom is cleared at the point that the wave elevation on the transom according to (4) equals the transom draft.

We remark here that a regression formula for the wave elevation at the transom in the wetted regime, derived in (Maki et al, 2005) from experimental data including 3D hull models, contains a speed dependence according to the function $Fn_{tr}^{1.966}$, again indicating a constant base pressure coefficient.

For model scale, we have derived the base pressure coefficient from the computed wave elevation on the transom, yielding a fairly constant value of *Cpbase = -0.23*. Now the 'jet-pump' effect is reduced by the presence of the boundary layer that is shed at the transom edge: the thicker the boundary layer, the smaller the pressure reduction. Hoerner (1957) gives an empirical relation $Cd_{base} = c / \sqrt[3]{Cfb}$ in which Cfb is the frictional drag coefficient for the body. If we accept the inverse third root proportionality and apply that to the ratio of frictional drags of model and full scale, from the Cpbase = -0.23 for model scale we obtain Cpbase = -0.29 for full scale, which is in good agreement with the computed wave elevation at the transom for full scale.

Fig. 19 then shows the resistance components found from this simple model. We have plotted the results here against the transom draft *ztr/L*. For low draft, $\zeta = z_{tr}$, and the resistance consists of the dry-transom contribution alone, which is quadratic in the transom draft. From a certain value, ζ remains constant, the excess transom draft forms a wetted part and the resistance consists of a constant hydrostatic contribution and a linear part due to the hydrodynamic pressure on the wetted part of the transom. For much of the range the agreement with the computed transom resistance (the markers) is striking. The approximate model thus seems to provide some understanding of the mechanism that leads to the scale effect in the wave elevation at the wetted transom; and of the dependence of the transom drag on the draft (or Fn_{tr}) and its scale effect.

We remark here that on the other hand, the assumption of a constant base pressure coefficient has limitations. When the transom is only just wetted, stern waves start building up. Thereby the flow leaving the transom curves upward, causing a further pressure reduction relative to the base flow mechanism (see the gradient markers in Fig. 19). Thus the simple constant-pressure base drag model does not apply any more, and the transom is cleared earlier than according to the model.

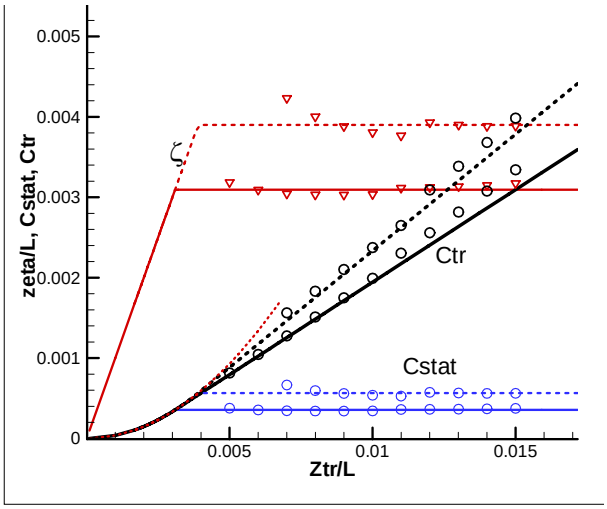

Figure 19: Wave elevation at the transom, and resistance, against transom immersion. Markers: from RANS computation; lines: simple model. Blue: *Cstat*; Black: *Ctr*. full lines: model scale; dashed lines: full scale.

DISCUSSION

In the present paper a flat-bottomed ship (backward facing step with free surface) has been used as a model for the flow off a transom. Although this has proven to be very useful, and to provide insight in the flow off a transom, it is not complete. Thus, a word of caution is in place regarding the application of the present results to practical ship design.

In the results presented in Fig. 10 a clear scale effect was found on the wave length and wave pattern aft of the transom. Moreover, large scale effects were found in the inception of stern wave breaking. However, it can be seen in Fig. 10 that the height of the first wave aft of the transom is greater at model scale than at full scale and in inviscid flow. This is in contradiction with the experience that inviscid-flow methods tend to over-predict the stern wave system of ships, usually attributed to the neglect of viscous effects. Since the present results are shown to be

accurate, it must be concluded that the flat-bottomed ship is not entirely representative of transom flow in practice, as it does not show this familiar viscous effect on the stern wave system.

Therefore some additional computations have been made, in which the aft end of the vessel was tapered with an angle of approximately three degrees. The draught of the plate equalled 0.25 metres. Figure 20 presents the corresponding wave profiles for inviscid flow, and for model and full-scale Reynolds number. In this figure a clear reduction of the height of the trailing wave system is found with decreasing Reynolds number, similar to what one would expect for ship stern flows. The difference with the flat-bottomed plate is that here there is a pressure rise towards the stern caused by the form of the vessel. The displacement effect of the boundary layer and wake reduces this pressure rise, resulting in a reduction of the wave amplitudes generated.

Although in this 2D test case it is a rather weak effect, this reduction of the stern wave height for model scale relative to full scale will tend to delay the onset of stern wave breaking on model scale, and thus leads to a scale effect contribution that is opposite to that which we found for the flat-bottomed ship. Consequently, the large scale effect on the critical Froude number observed in this study might turn out differently in actual 3D cases with more general shapes.

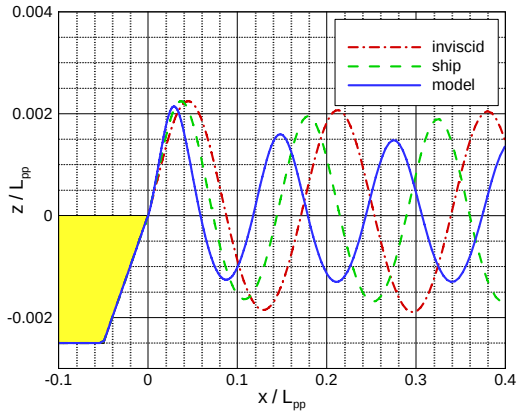

Figure 20: The scale effect on the wave system in the wake of a plate with a tapered end.

CONCLUSIONS

This study has addressed free-surface RANS computations for transom stern flows, considering the dry-transom, intermediate and wetted-transom regimes. We have considered a simple 2D test case, consisting of a barge-type vessel with horizontal bottom and vertical transom. Our main conclusions are:

- Using our surface-fitting RANS method in a steady formulation, and using the steady iterative solution algorithm for the free surface, it has appeared to be well possible to obtain accurate solutions for the transom flow, in both the dry-transom and wetted-transom regimes.
- The present method permits to obtain well-converged, numerically accurate steady results in a rather straightforward manner. Thus we have e.g. been able to accurately determine scale effects in the various regimes.
- In the intermediate regime, in which the transom is cleared but a spilling breaker occurs at the front of the following wave, it appeared to be harder to obtain a converged free surface, and at this moment only some rather coarse solutions have been obtained, which are qualitatively reasonable but not reliable yet.
- For the dry-transom regime, quasi-inviscid solutions have been computed with our method, which are in excellent agreement with the potential-flow solutions from Vanden-Broeck (1980), and also indicate the limiting value Fn_{tr} = 2.26 at which the stern waves reach maximum height.
- Viscous effects were found to reduce the trailing wave length, and more strongly for model scale than for full scale, due to the velocity defect in the wake.
- For increasing transom immersion, and consequently increasing steepness of the stern waves, the longitudinal velocity at the first wave crest decreases, and eventually it quickly falls to zero. This indicates the onset of stern wave breaking. In inviscid flow this happens for Fn_{tr} = 2.26, but for the viscous-flow cases considered here, this limit is shifted to about 3.3 for full scale, 4.0 for model scale. Therefore, a large scale effect is present on the inception of wave breaking, and in a range of transom immersions a spilling breaker will be present at model scale, but a smooth flow at full scale.
- Solutions obtained for the wetted-transom regime are in good agreement with the experimental data from Maki (2006), for the wave profile aft of the transom. Apparently, neglecting the unsteadiness of the flow observed in the experiments is not a serious omission in this regime.
- For wetted transoms, some scale effect was found on the wave elevation at the transom, and also on the occurrence of transom ventilation. In a small range of transom immersions, there will be a recirculation region at model scale, but the transom

is just cleared at full scale, with wave breaking occurring aft of the transom.

- Scale effects on the transom resistance were found, in the wetted regime only (for this case). For full scale the transom resistance coefficient is somewhat larger than for model scale.
- A simple transom flow model has been formulated, based on the assumption of a constant base pressure coefficient at the transom; which gives insight in the principal mechanism determining the wetted regime and its scale effects.
- The present test case provides very useful insights in the characteristics of transom flows and permits good validations. However, it does not display any influence of the displacement effect of the boundary layer and wake on the stern pressure distribution and trailing wave amplitude. This effect will, in more general 3D cases, partly counteract the large scale effect on the inception of stern wave breaking found in the present study.

ACKNOWLEDGEMENT

The permission of K. J. Maki to use his experimental data obtained at the University of Michigan is gratefully acknowledged.

REFERENCES

Banner, M.L. and Phillips, O.M., "On the incipient breaking of small scale waves", Journal of Fluid Mechanics, Vol. 65, part 4, 1974, pp. 647-656.

Duncan, J.H., "The breaking and non-breaking wave resistance of a two-dimensional hydrofoil", Journal of Fluid Mechanics, Vol 126, 1983, pp. 507-520.

Haussling, H.J., Miller, R.W. and Coleman, R.M. (1997), "Computation of high-speed turbulent flow about a ship model with transom stern", AMSE Fluids Eng. Division Summer meeting.

Hino, T. (editor), "CFD Workshop Tokyo", National Maritime Research Institute, Tokyo, Japan, March 2005.

Hoekstra, M., "Numerical simulation of ship stern flows with a space-marching Navier Stokes method", Thesis, Techn. Univ. Delft, October 1999.

Hoerner, S.F., "Fluid-dynamic drag", 1957.

Larsson, L., Stern, F. and Bertram, V. (eds.), "Gothenburg 2000 --- A workship on numerical ship hydrodynamics", Chalmers University, Gothenburg, Sweden, August 2000.

Lin, C.W. and Percival, S. (2001), "Free surface viscous flow computation around a transom stern ship by Chimera overlapping scheme", 23rd Symp. Naval Hydrodynamics, Val de Rueil, France.

Maki, K.J., "Transom stern hydrodynamics", Thesis, University of Michigan, 2006.

Maki, K.J., Doctors, L.J., Beck, R.F. and Troesch, A. (2005), "Transom-stern flow for high-speed craft", 8th Int. Conf. on Fast Sea Transportation, FAST 2005, Saint Petersburg, Russia.

Maki, K.J., Iafrati, A., Rhee, S., Beck, R. and Troesch, A. (2006), "The transom stern modeled as a backward facing step", 26th Symp. Naval Hydrodynamics, Rome, Italy.

Menter, F.R., "Eddy-viscosity transport equations and their relation to the k-ε model", Journal of Fluids Engineering, Vol. 119, pp. 876-884, 1997.

Menter, F.R., "Two-equation eddy-viscosity turbulence models for engineering applications", AIAA Journal, Vol. 32, August 1994, pp. 1598-1605.

Raven, H.C. (1998), "Inviscid calculations of ship wavemaking --- capabilities, limitations and prospects", 22nd Symp. Naval Hydrodynamics, Washington D.C.

Raven, H.C. and Starke, A.R., "Efficient methods to compute ship viscous flow with free surface", 24th Symp. Naval Hydrodynamics, Fukuoka, Japan, 2002.

Raven, H.C. and Van Brummelen, E.H., "A new approach to computing steady free-surface viscous flow problems", 1st MARNET-CFD workshop, Barcelona, Spain, 1999.

Raven, H.C., Van der Ploeg, A., and Starke, A.R. (2004), "Computation of free-surface viscous flows at model and full scale by a steady iterative approach", 25th Symp. Naval Hydrodynamics, St.John's, Canada.

Saunders, H. (Ed.), "Hydrodynamics in Ship Design", Vol. 2, pp. 529-531, Society of Naval Architects and Marine Engineers, 1957.

Schmidt, G.H., "Linearised stern flow for a two-dimensional shallow-draft ship", Journal of Ship Research, Vol. 254, 1981.

Scorpio, S.M. and Beck, R.F. (1997), "Two-dimensional inviscid transom stern flow", 12th Int. Workshop on Water Waves and Floating Bodies, Carry le Rouet, France.

Van Brummelen, E.H., Raven, H.C. and Koren, B., "Efficient numerical solution of steady free-surface Navier-Stokes flow", Journal of Computational Physics, Vol. 174, 2001, pp. 120-137.

Van der Ploeg, A., Eça, L. and Hoekstra, M., "Combining accuracy and efficiency with robustness in ship stern flow calculation", 23rd Symp. Naval Hydrodynamics, Val de Rueil, France, Sept. 2000.

Vanden-Broeck, J.–M., "Nonlinear stern waves", Journal of Fluid Mechanics, Vol. 96, part 3, 1980, pp. 603-611.

Wilson, W., Fu, T.C., Fulleton, A. and Gorski, J. (2006), "The measured and predicted wave field of model 5365: An evaluation of current CFD capability", 26th Symp. Naval Hydrodynamics, Rome, Italy.